SQUEEZE FILM DAMPER BEARING EXPERIMENTAL *VS* ANALYTICAL RESULTS FOR VARIOUS DAMPER CONFIGURATIONS

by

Mark J. Kuzdzal

Development Engineer

and

Jerry F. Hustak

Manager Engineering Sciences

Dresser-Rand

Turbo Products Division

Olean, New York

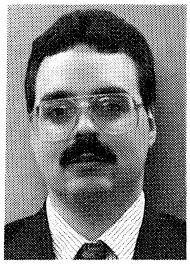

Mark J. Kuzdzal is a Product Development and Rotordynamics Engineer at Dresser-Rand's Turbo Products Division in Olean, N.Y. He has been employed there since obtaining his B.S. degree (Mechanical Engineering) from the State University of New York at Buffalo (1988). Mr. Kuzdzal's major focus is on product development with emphasis on squeeze film damper bearings. He has applied for one U.S. patent and has coauthored three technical papers.

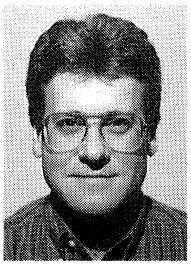

Jerry Hustak is the Manager of Engineering Sciences for Dresser-Rand's Turbo Products Division. He has worked in the turbomachinery field for the past 17 years. Prior to joining Dresser-Rand, he held the position of Analytical Engineer at Ingersoll-Rand working in the area of Rotordynamics. He started his career at Transamerica Delaval on an Engineering Management Training Program where he held positions in Marketing, Test Engineering, Field Service and Compressor Design. Mr. Hustak has a Bachelor's degree (Mechanical Engineering) from the Pennsylvania State University. He has authored eight technical papers and holds one patent.

ABSTRACT

Higher speeds, longer shafts, and increased power has made squeeze film damper (SFD) bearing performance increasingly more important to control both synchronous and subsynchronous vibration in rotating machinery. SFD bearing performance from a ten stage high pressure barrel centrifugal compressor that has been specifically modified for SFD bearing development is presented. SFD bearing performance is investigated for both synchronous unbalance response and rotordynamic instability. A comparison is made of experimental and analytical results for a hydrodynamic five shoe tilt pad bearing supported by an O ring centered damper (eccentricity, e = 0.0 and e = 0.6), mechanically spring centered damper (e = 0.0 and e = 0.8), a bottom resting damper (e = 1.0), and a standard nondamper (rigid support). The results of the tests clearly show that a properly designed SFD is an effective means of reducing the severity of critical speeds and improving the stability threshold of rotor bearing systems.

INTRODUCTION

This presentation is broken down into three major sections. The first section includes a description of the test vehicle, terminology, experiments completed and damping approximation techniques. The rig is driven through a gear box by a variable speed induction motor at speeds from slow roll to 10,000 rpm. The shaft has been designed to be very flexible, which allows the testing to include high amplification factors and low stability thresholds. There are provisions to apply unbalance at various locations in the test vehicle and labyrinth seals are specifically designed to drive the rotor unstable at the first natural frequency while the rotor operates at maximum speed.

The second section discusses experimental *vs* analytical midspan synchronous unbalance response predictions as a function of stiffness and damping. A direct comparison of experimental and analytical results is made for the first natural frequency location and amplification factor. Experimental results are obtained from vibration probes that monitor shaft motion at the bearings, midspan and quarterspan locations. Additionally, proximity probes are installed to monitor SFD bearing cage motion relative to ground.

Experimental results are presented in the form of bodé plots for all the different SFD bearing configurations tested. These plots graphically show, for the same unbalance, large variations in vibrations signatures with different SFD configurations.

The final section compares the system stability threshold relative to variations of pressure, destabilizing forces and rotational speed. A description of the labyrinth seal destabilizing mechanism in the rig along with analytical predictions of the labyrinth seal excitation is presented. Calculations of the rotor systems logarithmic decrement as a function of aerodynamic excitation for various damping values and a damper optimization study are presented.

Using analytical predictions, a seal was designed to purposely destabilize the rotor. Variations in pressure differential across the labyrinth seals demonstrate a parametric study of rotor instability *vs* damper bearing design. Additionally, experimental comparisons between a nondamper and an SFD showed the damper bearing significantly improved the stability threshold of the rotor bearing system. A comprehensive comparison is made between analytical and experimental results.

EXPERIMENTAL TESTING AND TERMINOLOGY

Damper Bearing Development Rig

The damper bearing development rig is used to validate and calibrate theoretical predictions of various damper bearing designs. A photograph of the rig showing the motor, gear and compressor is shown in Figure 1. This development rig is a 10 stage high pressure

barrel compressor with 4.0 inch journal bearings and a 62.938 in bearing span as shown in Figure 2. Impellers are simulated with disks (dummy impellers) to reduce windage allowing operation without the need of complicated testing loops. All the nonrotating internal components typically found in a centrifugal compressor were removed for ease of testing. Nitrogen is introduced through the compressor head which purges oxygen from the case, removes heat, and acts as an aerodynamic excitation as it leaves the case through labyrinth seals.

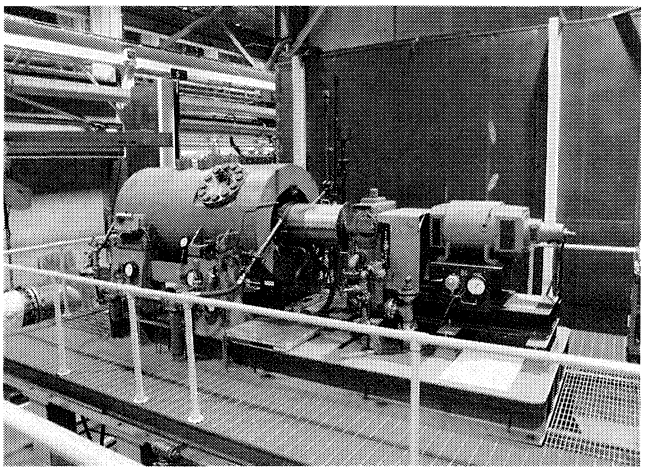

Figure 1. The Development Rig.

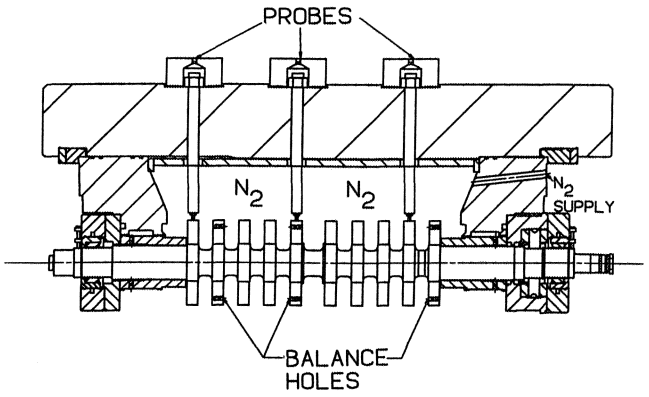

Figure 2. Cross Sectional Drawing Showing Rig Internals.

The shaft has been undercut between the impellers to 3.5 in, which produces a very flexible rotor. An undamped critical speed analysis shows the rotor's rigid bearing first natural frequency is one fourth the maximum continuous speed (Figure 3). Undercutting the shaft drops the stability threshold of the rotor and increases the amplification factor (AF) of the first natural frequency. The highly flexible rotor accentuates the performance of a damper bearing and demonstrates the differences in rotor vibration levels as a function of various damper bearing designs.

Unbalance Location Capabilities

The damper bearing rig has provisions for application of unbalance weights to the rotor without disassembly of the case. The second, fifth and tenth impellers have holes drilled and tapped into them near their outer diameter to accept unbalance weights as shown in Figure 2. This allows for midspan and quarterspan out of phase unbalance configurations. Additionally, coupling unbalance can be applied to the rig. The testing program includes testing each

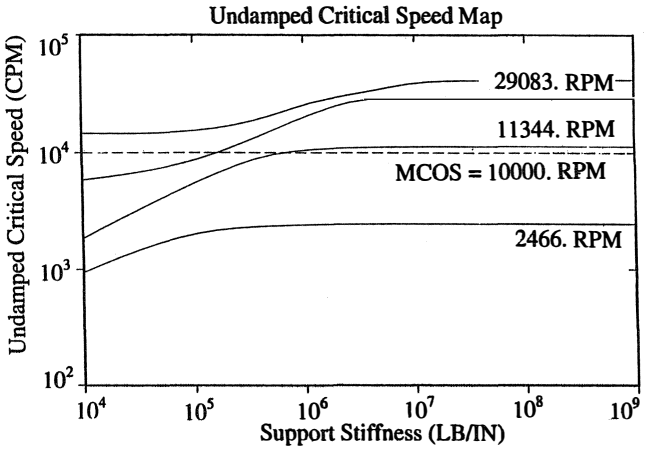

Figure 3. Undamped Critical Speed Map.

bearing design with three magnitudes of weight at the midspan, quarterspan and coupling location. Hence, each bearing design is subject to nine different unbalance conditions. For comparison purposes, the same unbalance weights have been applied in the same unbalance locations to provide consistent unbalance forces for all the designs tested.

Subsynchronous Excitation Mechanism

Nitrogen is introduced into the case through the drive end head. The nitrogen bathes the rotor and leaks out of the case through labyrinth seals that are located just outboard of the first and last disks as shown in Figure 2. The nitrogen is forced down the face of the disk into an axial chamber between the rotating shaft and non-rotating labyrinth. A closeup view of this axial chamber is shown in Figure 4. For the first 5.375 in under the seal, the shaft has been roughened by a knurling process while the inside diameter of the labyrinth has been machined smooth. The roughened shaft and smooth labyrinth act to add tangential velocity to the nitrogen as it passes through the labyrinth. The nitrogen, flowing through the seal is the mechanism that drives the rotor unstable at its first natural frequency. Due to pressure limitation, the maximum seal pressure differential tested to date is 85 psi. The magnitude of the destabilizing force is controlled by the pressure differential across the seal; the higher the pressure differential, the greater the destabilizing force.

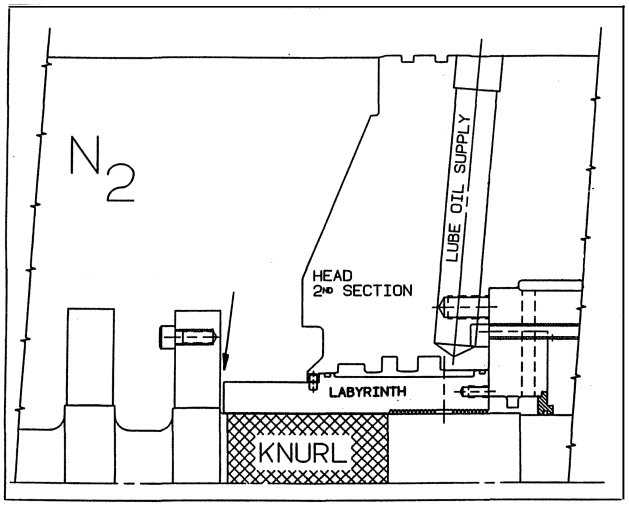

Figure 4. Cross Sectional Drawing Showing Details of Labyrinth Seal.

Damper Bearing Terminology

The terminology used to describe the squeeze film damper and tilt pad bearing assembly is shown in Figure 5. The cage is a solid ring that holds the tilt pad shoes in place. The housing is bolted to the compressor head and is considered the ground reference frame (i.e., zero vibration). Vibration probes are mounted on the housing outboard of the radial bearings. A damper bearing is created when a clearance is made between the cage and the housing. Oil flows through the housing into the SFD clearance chamber, which is sealed on both ends with O-rings, and into the cage. When the O-rings are used to keep the cage centered relative to the housing, the damper is called an O-ring centered damper. When the load carrying capacity of the O-ring is insufficient to support the static load of the shaft and cage, the cage rests on the bottom of the housing. This type of damper is called a bottom resting damper.

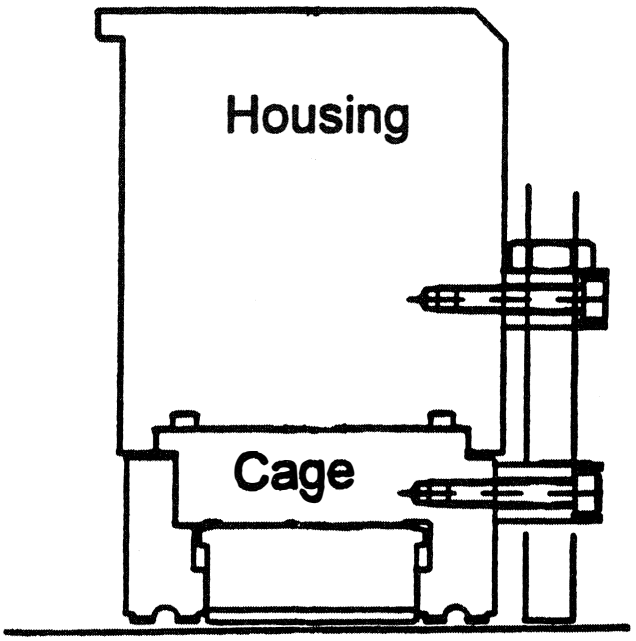

Figure 5. Cross Sectional Drawing Showing Details of SFD Bearing.

Additionally, two different kinds of mechanical centering damper designs were investigated. These consisted of a mechanical arc spring and a hanging spring assembly are shown in Figure 6. These two devices are used to support the gravity load of the rotor and the cage while centering the cage in the housing. They are both shown on the same figure to minimize art work, but are not designed to operate in the same assembly.

The first type of mechanical arc spring has a semicircular profile with hooks on both ends. The spring fits into a circumferential relief groove in the bottom half of the housing and is supported with hooks at the horizontal split. Clearance is maintained between the spring and the housing except in the hook area. At bottom dead center, the inside radius of the spring has a raised land which contacts the cage and provides support in the vertical direction. The spring is designed to have a predetermined spring rate and is preloaded to offset half the rotor weight when the cage is centered in the housing. Vertical damper stiffness is a combination of the mechanical spring and the O-ring end seals while horizontal stiffness come from the O-rings alone.

The second type of mechanical spring damper assembly consists of two bolts and belleville washers (Figure 7). The bolts are threaded into the cage and are free to move in a clearance hole in

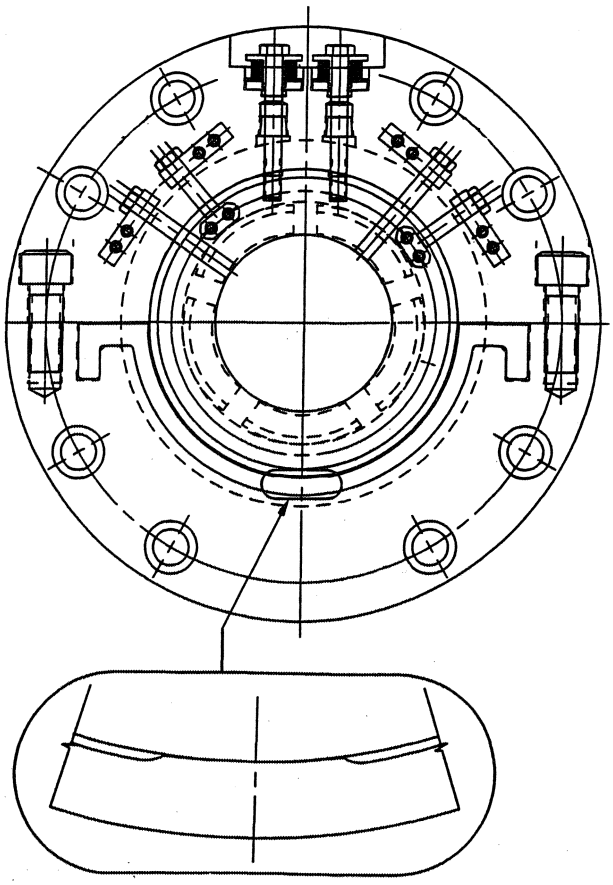

Figure 6. Drawing Showing SFD Spring and Probes Assemblies.

the housing. Belleville washers placed under the bolt heads provide vertical spring stiffness for the cage. Stiffness values are adjusted by changing the orientation and number of spring washers (i.e., parallel and/or series). Spring preload, which allows soft springs to carry heavy loads and still center the cage in the housing, is adjusted by turning the bolts. This design allows testing the cage at various eccentricity ratios while holding the damper spring rate approximately constant.

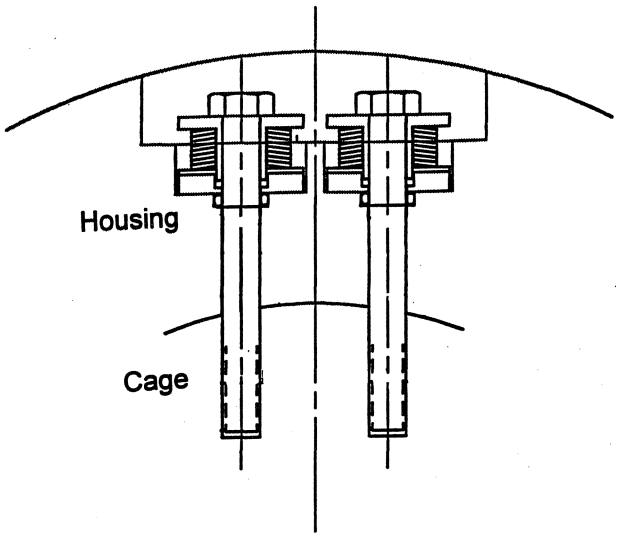

Figure 7. Drawing Showing SFD Hanging Spring Design.

Instrumentation

The test vehicle has vibration probes located at the bearings, midspan, and quarterspan points of the rotor. There are two pairs of probes at each bearing. One set monitors journal motion relative to ground while the second set monitors damper bearing cage motion relative to ground as shown in Figure 6. Additionally, three pairs of probes are located internal to the casing as shown in Figure 2. The first pair is located at the midspan of the rotor and the next two pairs are located at the quarterspan of the rotor (i.e., at the first, fifth and ninth impellers). Axial position is measured by an axial probe located on the free end of the rotor.

Bearing Configurations Tested

The bearing configurations tested are shown in Table 1.

Table 1. Damper Bearing Configurations Tested.

Bearing Configuration	Damper Stiffness K (lb/in)	Damper damping C (lb-sec/in)	Eccentricity ratio - e (dim.)	Cage relative to housing location
Standard Non-damper	Rigid	0	0	Centered
O-ring Damper 90 Duro. viton	60,000	600	0	Centered
O-ring Damper 90 Duro. aflas	155,000	1,200	0.6	Cage 3 mils above housing centerline
O-ring Damper 75 Duro. viton	30,000	1,200	0.6	Cage 3 mils below housing centerline
Bottom Resting Damper 75 Duro. viton	Rigid	10,000+	1.0	Cage 5 mils below housing centerline
Arc Spring Damper 75 Duro. viton	65,000	600	0	Centered
Hanging Spring Damper 75 Duro. viton	90,000	600	0	Centered
Hanging Spring Damper 75 Duro. viton	90,000	3,000	0.8	Cage 4 mils above housing centerline

Damping Approximation Techniques

Damping is approximated using a non-cavitated oil film calculation as shown in Equation (1).

$$C = (mu)(pi)4D(l/d)^3L \quad (1)$$

Where:
C = Damping (lb-sec/in)
mu = Viscosity (lb-sec/in^2)
pi = 3.14159
D = Cage outer diameter (in)
l = Active damper length (in)
d = Diametrial clearance (in)
L = Eccentricity coefficient = $1/(1-e^2)^{2/3}$
e = Eccentricity ratio (dim)

The eccentricity coefficient (L) is one when the cage is perfectly centered in the housing (e = 0.0). As the cage becomes more eccentric in the housing the value of L goes up exponentially as shown in Figure 8. Typically a damping value is calculated for a centered damper then augmented by the value of L. As the cage becomes more eccentric in the housing calculated damping of the assembly increases [1]. The 90 durometer aflas and the 75 durometer viton O-ring centered dampers had an eccentricity ratio of approximately 0.6. Based on the adjustment shown in Figure 8, the value of L is two, and the actual damping expected in the system could be twice the calculated amount for a centered damper. The effect of changes in SFD damping *vs* cage eccentricity relative to the housing is shown in Table 2. The damper configurations tested showed large variations in both synchronous and subsynchronous vibration characteristics, which will be extensively covered herein [2].

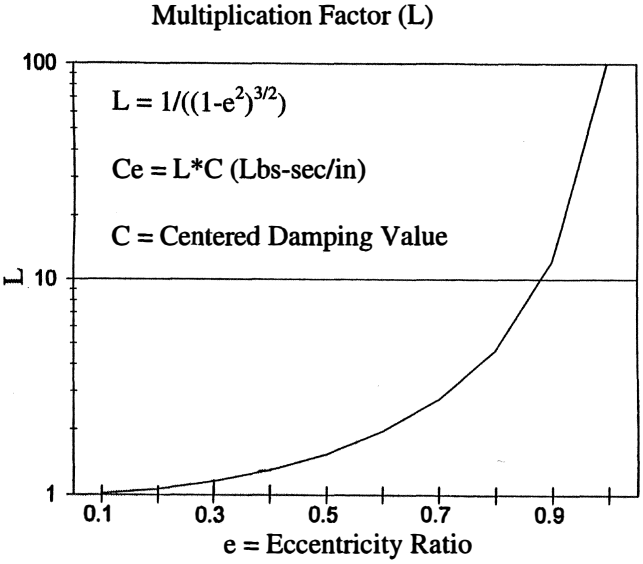

Figure 8. Eccentricity Ratio Vs *Damping Multiplication Factor.*

Table 2. Comparison of the Cage Location for Dampers Tested.

Type	Calculated Damping (lb-sec/in)	Cage location
90 Durometer viton	600.	e=0.0
Arc Spring	600.	e=0.0
Hanging Spring	600.	e=0.0
90 Durometer aflas	1200.	e=0.6
75 Durometer viton	1200.	e=0.6
Hanging Spring	3000.	e=0.8
Bottom Resting	10,000.+	e=1.0

ANALYTICAL SYNCHRONOUS UNBALANCE RESPONSE

Analytical models of the rotor/bearing system were constructed and used to conduct a synchronous unbalance response study. The analysis tools used were a version of the original Lund unbalance response program and a tilt pad bearing code [3]. During the synchronous unbalance response testing, the seals were held at a differential pressure of 15 psi. With this small pressure differential, the labyrinth seals have minimal influence on the synchronous unbalance response study. The effects of the labyrinth seals were not included in the synchronous unbalance response analysis.

Testing was conducted using midspan, quarterspan and coupling unbalance configurations. For the purposes of determining synchronous unbalance response performance of various SFD bearing configurations, a midspan unbalance will be used for this discussion. This was chosen to illustrate the difference in vibration

amplitudes and amplification factors going through the first critical speed. The results of the quarterspan and coupling unbalance will not be discussed.

The analytical results for this rotor with various SFD stiffness and damping coefficients is shown in Figures 9, 10, and 11 for a 3.0 oz/in midspan unbalance. To demonstrate the effect of the damper bearing stiffness on synchronous unbalance response, damping was held constant and stiffness was varied as shown in Figure 9 and summarized in Table 3. A parametric study was made holding stiffness constant at 50,000 lb/in and varying damping, as shown in Figure 10, and summarized in Table 4. Another parametric study is shown in Figure 11, and summarized in Table 5, for holding stiffness constant at 100,000 lb/in and varying damping.

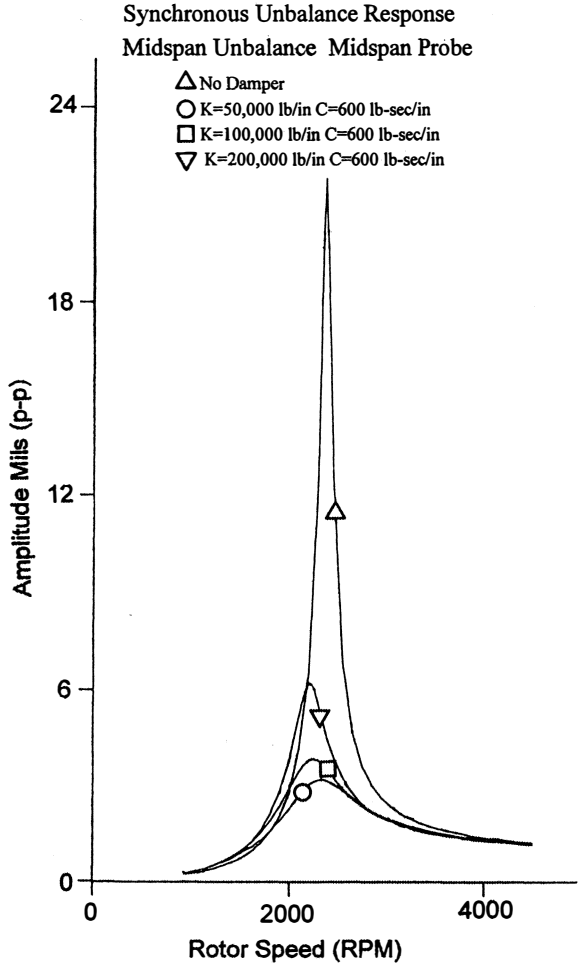

Figure 9. Analytical Rotor Response as a Function of SFD Stiffness (c = 600 lb-sec/in).

Table 3. Analytical Synchronous Unbalance Results for Constant Damping Vs *Stiffness.*

Stiffness (lb/in)	Damping (lb-sec/in)	NC1 (rpm)	Midspan A.F.
No Damper	-	2375.	22.2
50,000	600.	2325.	2.8
100,000	600.	2250.	3.5
200,000	600.	2225.	6.1

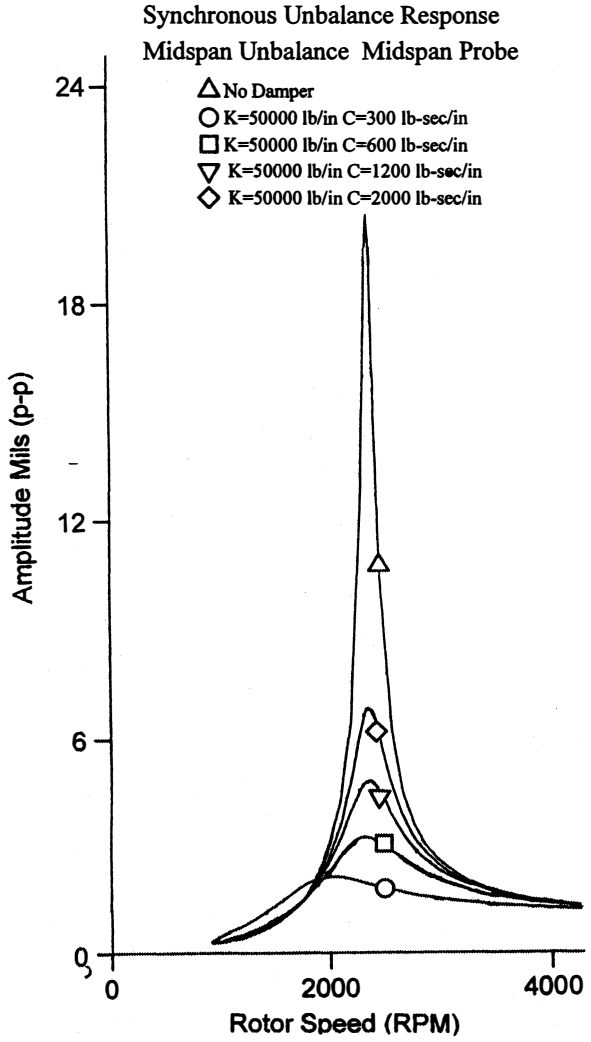

Figure 10. Analytical Rotor Response as a Function of SFD Damping (K = 50,000 lb/in).

Table 4. Analytical Synchronous Unbalance Results for Stiffness of 50,000 lb/in Vs *Damping.*

Stiffness (lb/in)	Damping (lb-sec/in)	NC1 (rpm)	Midspan A.F.
No Damper	-	2375.	22.2
50,000	300.	2025.	1.95
50,000	600.	2325.	2.8
50,000	1200.	2350.	4.6
50,000	2000.	2360.	6.75

For a SFD with a stiffness between 50,000 to 100,000 lb/in, analytical predictions indicate a damping value of approximately 600 lb-sec/in would represent the optimum SFD bearing characteristics for this rotor assembly based on minimizing amplification factors and synchronous vibration levels through the first natural frequency. As damping is increased beyond 600 lb-sec/in, the midspan amplitude at the first natural frequency increases as shown in Tables 6 and 7. As will be demonstrated later herein, the

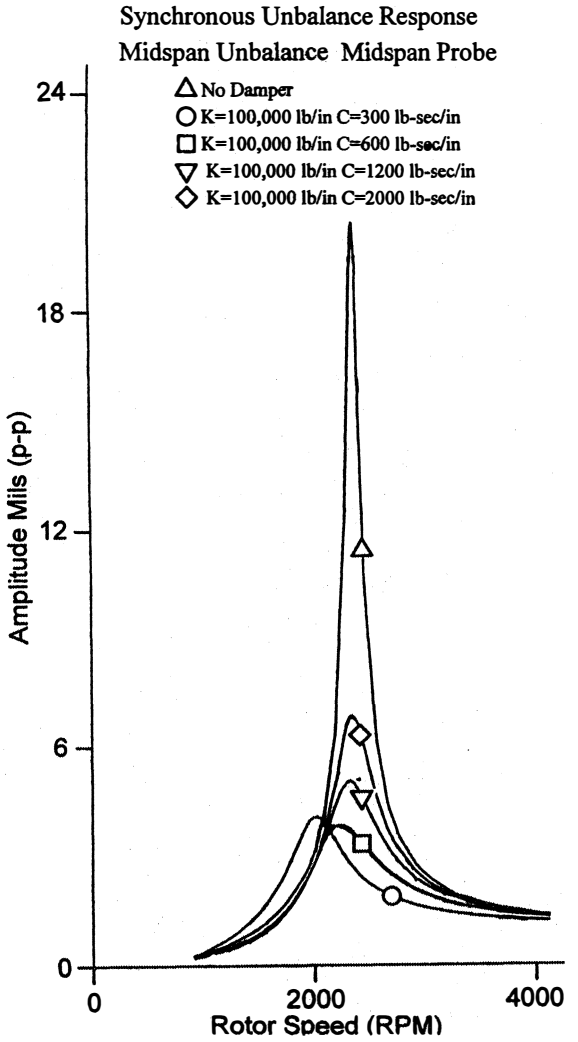

Figure 11. Analytical Rotor Response as a Function of SFD Damping (K = 100,000 lb/in).

test results support the theoretical predictions that increased damping can be achieved with a non centered cage.

Analytically, for a SFD with a stiffness value between 50,000 to 100,000 lb/in, damping values greater than 2,000 lb-sec/in are required to achieve two times the amplitude of a centered damper at the first natural frequency. This corresponds to SFD eccentricity ratios above about 0.7 (Figure 8).

SYNCHRONOUS VIBRATIONS TEST RESULTS

Each of the SFD bearing configurations previously mentioned were subject to identical unbalance forces. The unbalance test results presented herein are for a 3.0 oz/in (17.4 grams at 4.875 in radius) unbalance at the rotor midspan. Test results for the midspan horizontal probe, free end cage horizontal motion relative to ground and free end journal horizontal motion relative to ground are presented by plotting amplitude *vs* speed for each SFD configuration. Test results presented are limited to the free (non-drive) end of the rotor for the sake of brevity.

Exploring the midspan horizontal probe shows large variations in amplitude and amplification factors for the dampers tested. The 90 durometer viton O-ring center damper and the arc spring supported damper performed very well with low amplification factors and low overall midspan amplitudes, as shown in Figure 12.

Table 5. Analytical Synchronous Unbalance Results for Stiffness of 100,000 lb/in Vs *Damping.*

Stiffness (lb/in)	Damping (lb-sec/in)	NC1 (rpm)	Midspan A.F.
No Damper	-	2375.	22.2
100,000	300.	2025.	7.0
100,000	600.	2250.	3.4
100,000	1200.	2325.	4.8
100,000	2000.	2350.	6.8

Table 6. Analytical Synchronous Amplitude Vs *Damping at 50,000 lb/in Stiffness.*

Stiffness (lb/in)	Damping (lb-sec/in)	Midspan Amp. (mils p-p)	Amplitude Increase
50,000.	C=600.	3.0	1.0X
50,000.	C=1200.	4.8	1.6X
50,000.	C= 2000.	6.6	2.2X
No damper	-	20.4	6.8X

Table 7. Analytical Synchronous Amplitude Vs *Damping at 100,000 lb/in Stiffness.*

Stiffness (lb/in)	Damping (lb-sec/in)	Midspan Amp. (mils p-p)	Amplitude Increase
100,000.	C=600	3.6	1.0X
100,000.	C=1200	5.1	1.4X
100,000.	C= 2000	7.2	2.0X
No damper	-	20.7	5.7X

Both of these dampers had cage eccentricity values close to zero, which corresponds to calculated damping values of near 600 lb-sec/in. Static bench tests were conducted to determine force *vs* deflection values of the damper centering mechanism. Test results indicate damper stiffness values of 60,000 to 65,000 lb/in. The synchronous unbalance response analysis work presented shows a damper designed with these stiffness and damping characteristics is close to the optimum for minimizing the unbalance response through the first natural frequency.

The hanging spring SFD, with an eccentricity ratio of zero, has a calculated centered damping value of 600 lb-sec/in and a damper stiffness of 90,000 lb/in based on static push tests. This design performed well with low amplification factors and low overall midspan amlitudes (Figure 13).

The 75 durometer viton O-ring centered SFD which has the cage sitting low in the housing (e = 0.6), and the 90 durometer aflas O-ring centered SFD, which has the cage sitting high in the housing (e = 0.6), showed higher midspan horizontal vibration amplitudes and AFs than the centered dampers. Based on the damper calculation previously described, adjustments for eccentricity of 0.6 results in predicted damping values twice the center damping value or approximately 1400 lb-sec/in. Static bench test stiffness values for the 75 durometer viton and the 90 durometer aflas O-rings are approximately 30,000 lb/in and 155,000 lb/in. Even though these two damper designs have the same damping values, the difference in stiffnesses may account for the variation in synchronous unbalance response.

A bottom resting O-ring damper bearing (e = 1.0) performed slightly worse than the two SFD bearing previously mentioned

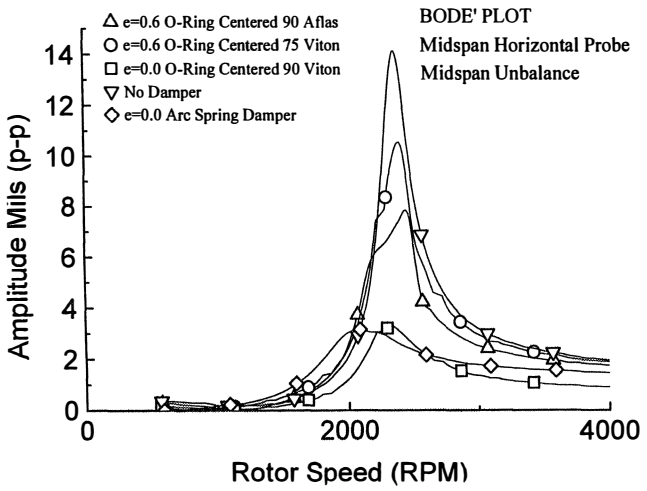

Figure 12. First Half Test Rotor Response Midspan Horizontal Probe.

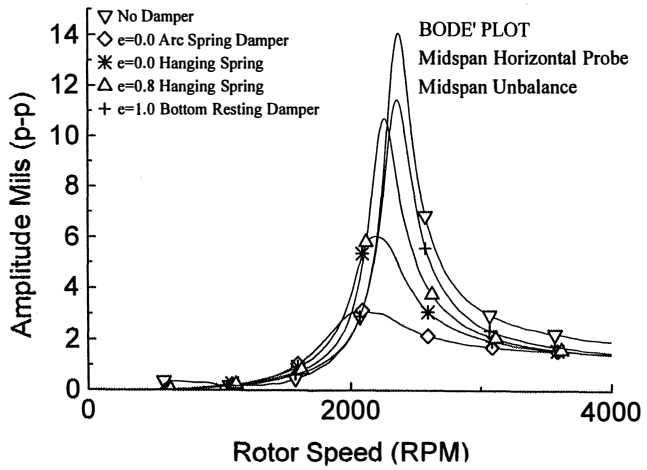

Figure 13. Second Half Test Rotor Response Midspan Horizontal Probe.

with an eccentricity ratio of 0.6. Additionally, the hanging spring SFD with an eccentricity ratio of 0.8, cage sitting high in the housing, performed similarly to the bottom resting damper.

The standard nondamper bearing had the highest midspan horizontal vibration and amplification factor of all the bearing designs tested. A summary of midspan probe test results with a 3.0 oz/in midspan unbalance is shown in Table 8.

Table 8. Summary of Synchronous Unbalance Response Test Results.

Damper Configuration	Eccentricity Ratio e (dim)	NC1 (rpm)	Midspan Amplitude at NC1 (mil p-p)	Amp. Factor (dim)
No damper	-	2370	14.1	11.9
Bottom Resting	1.0 (low)	2350.	11.4	12.0
75 viton O-ring	0.6 (low)	2400.	10.5	10.1
90 aflas O-ring	0.6 (high)	2450.	7.8	6.6
90 viton O-ring	0.0	2100.	3.3	5.2
Arc Spring	0.0	2080.	3.1	2.9
Hanging Spring	0.0	2250.	6.0	5.5
Hanging Spring	0.8 (high)	2300.	10.8	10.9

The response is shown in Figures 14 and 15 of the bearing cage motion relative to the ground for each assembly tested. The trend indicates that the more the SFD cage moves in the housing, the lower the midspan vibrations. For example, the mechanical arc spring SFD bearing showed the most cage vibration and minimized the amplitude and amplification factor of the first natural frequency at the midspan location. The converse of this is true for the hanging spring damper with a cage eccentricity of 0.8. Very little cage motion was seen and high midspan amplitudes resulted.

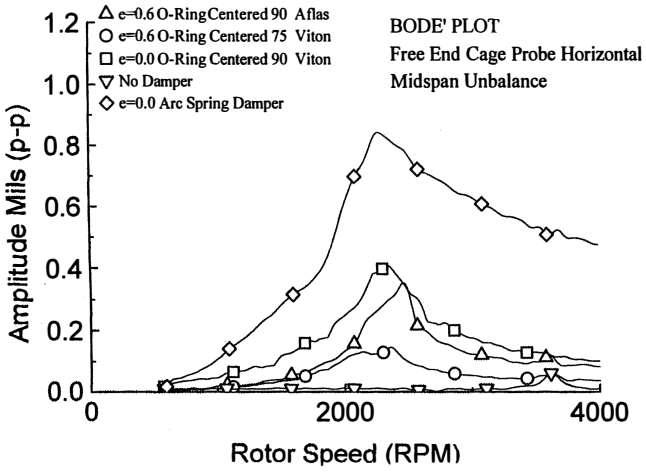

Figure 14. First Half Test Rotor Response Free End Cage Horizontal Probe.

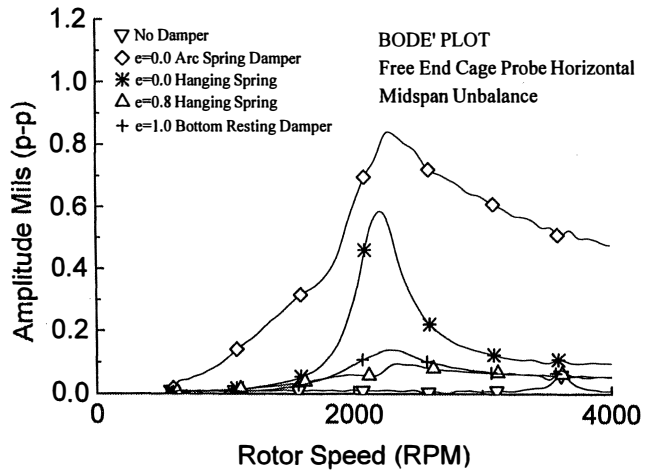

Figure 15. Second Half Test Rotor Response Free End Cage Horizontal Probe.

The final two bodé plots, Figures 16 and 17, show the rotor motion relative to ground at an axial location just outboard of the bearing centerline. This would be typical of the actual vibration probes on a production compressor. It has been shown that moderate amounts of cage motion is required to reduce the midspan vibration amplitude. This translates into higher overall amplitude levels at the journals of the compressor as shown in Figures 16 and 17. If minimizing the journal probe amplitude is the only consideration given during the design phase, the overall mechanical integrity of the system could be in jeopardy. There may be large amplitudes at midspan causing damaging rubs while the journal probe amplitudes indicate low vibrations passing through the first natural frequency. Such is the case of the standard nondamper bearing. While passing through the first natural frequency,

the non-damper bearing shows the lowest vibration amplitude at the journal location but has the highest amplitude at midspan. During the design of a rotordynamic system, compromises must be made to allow for larger amplitudes at the journal location to minimize the amount of amplitude at the midspan of the rotor. A summary of test results showing the first natural frequency, amplification factor and vibration levels all measured at the midspan is included in Table 8. By examining Table 8, it can be seen that the amplification factor is directly related to the midspan amplitude while passing through the first natural frequency.

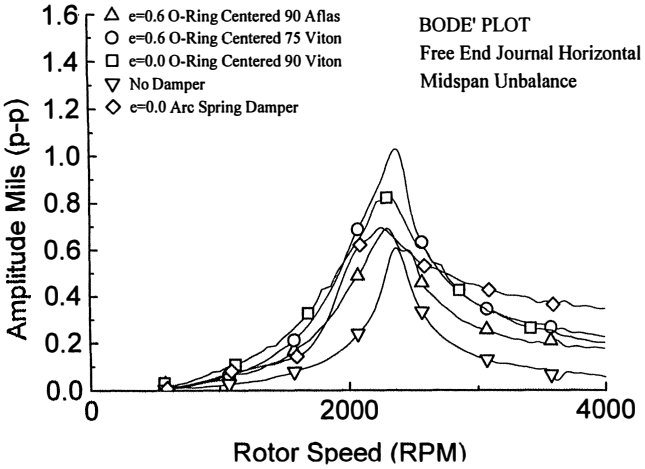

Figure 16. First Half Test Rotor Response Free End Journal Horizontal Probe.

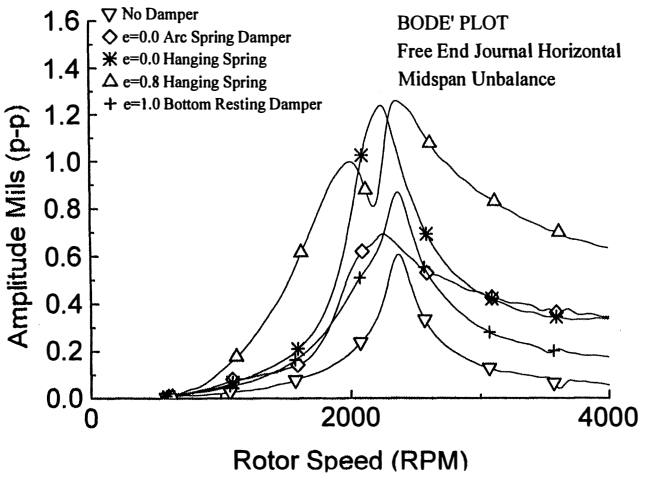

Figure 17. Second Half Test Rotor Response Free End Journal Horizontal Probe.

SUMMARY OF SYNCHRONOUS UNBALANCE RESPONSE RESULTS/CONCLUSIONS

The first and most general conclusion is the arc spring SFD bearing (e = 0.0) shows the most cage motion and the least midspan amplitude at the first natural frequency. Generally, the lower the cage motion the higher the amplification factor of the first natural frequency. An O-ring centered SFD bearing that has the cage centered relative to the housing (e = 0.0) has essentially the same synchronous unbalance response as an arc spring damper. It appears that, regardless of the centering method, a centered SFD with attributes that match the rotor's optimum stiffness and damping works very well for controlling synchronous vibrations. A properly centered damper reduced midspan amplitudes by a factor of five relative to a standard non damper bearing.

Secondly, the unbalance response program and the theory that predicts damping increases as cage eccentricity increases was supported by the data generated using the test rig.

Finally, when the rotor is passing through its first natural frequency, test results show that reduced amplitudes at the journal locations of the rotor may not be a good indicator of the amplitudes at the center of the rotor.

ANALYTICAL DESTABILIZATION FORCES

A knurled shaft section and a labyrinth seal were designed to provide the excitation or destabilizing mechanism used in the SFD bearing test rig. A description of the seal destabilizing mechanism was previously discussed and a cross section is shown in Figure 4 [4]. An analytical model of this labyrinth was built to conduct calculations to determine the stiffness and damping values generated by the labyrinth seal [5]. The labyrinth seal is comprised of both the tooth portion and the smooth portion. An attempt was made to analytically model the cavity between the knurled section of the shaft and the smooth portion of the labyrinth. The purpose of this cavity is to add tangential velocity to the nitrogen prior to entering the labyrinth teeth. The calculation method used has provisions for describing the roughness of the shaft through a variable called a Yamada coefficient (YNR). A Yamada coefficient of 0.079 is recommended for a smooth shaft [6, 7]. Unfortunately, the authors were unable to find any other information regarding how this coefficient changes as a function of shaft surface finish. Based on the SFD bearing rig, results show that as the differential pressure across the seal increases, the frequency of the subsynchronous vibrations does not appear to change very much.

Furthermore, analytical results show that a YNR of approximately 0.4 corresponds to a labyrinth direct stiffness (combined stiffness from both tooth and smooth portion of the seal) that does not change as a function of pressure as shown in Figure 18. Based on this assumption, the Yamada coefficient is estimated to be close to 0.4. At this YNR value the analysis predicts a value of direct stiffness close to zero.

The cross coupled stiffness and direct damping, which are both strong functions of the Yamada coefficients and the pressure across the seal, were calculated at YNR = 0.4. Labyrinth seal damping *vs* YNR is plotted in Figure 19 for various pressures across the seal. Labyrinth seal cross coupled stiffness *vs* YNR is plotted in Figure 20 for various pressures across the seal. Both of these plots show direct damping and cross coupled stiffness increase as YNR and seal pressure differential increase, however each has an opposite effect on the rotor from a destabilization view. The cross coupled stiffness is a destabilizing term and the direct damping is a stabilizing term.

The relationship between the two can best be described in Equation (2).

$$Q_{eff} = K_{xy} - C_{xx}(W) \qquad (2)$$

Where:

Q_{eff} = Effective Aero Cross Coupled Stiffness (lb/in)
K_{xy} = Cross coupled stiffness (lb/in)
C_{xx} = Direct damping (lb-sec/in)
W = Rotor whirl frequency (240.8 rad/sec)

The labyrinth seal effective aero cross coupled stiffness (Q_{eff}) *vs* shaft surface finish is shown in Figure 21 for various pressures across the seal. Because the K_{xy} value is larger than the C_{xx} (W) term, the effective aero cross coupled stiffness is positive and destabilizing. Furthermore, as the pressure across the seal is increased the destabilizing mechanism is increased. The calculated destabilizing aerodynamic cross coupled force was then used in a

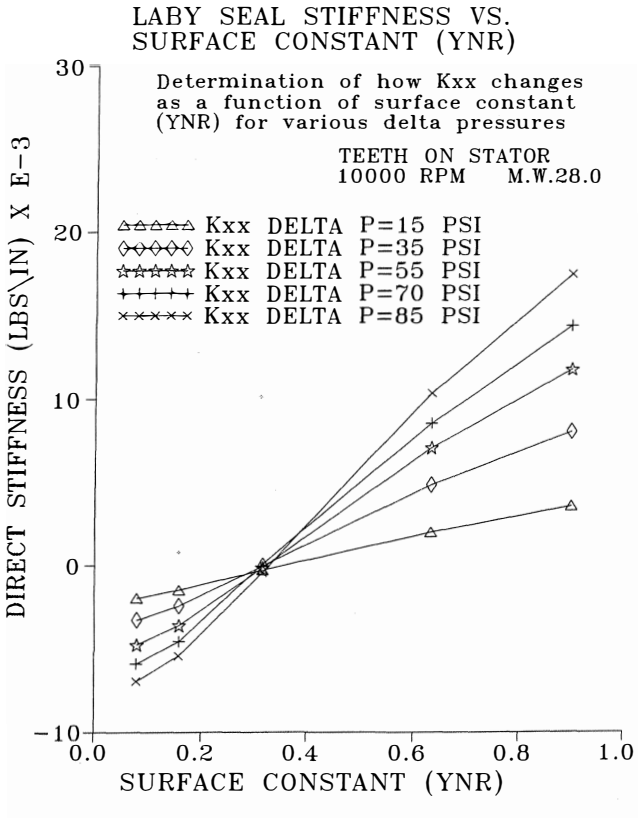

Figure 18. Labyrinth Seal Direct Stiffness Vs *Shaft Surface Constant.*

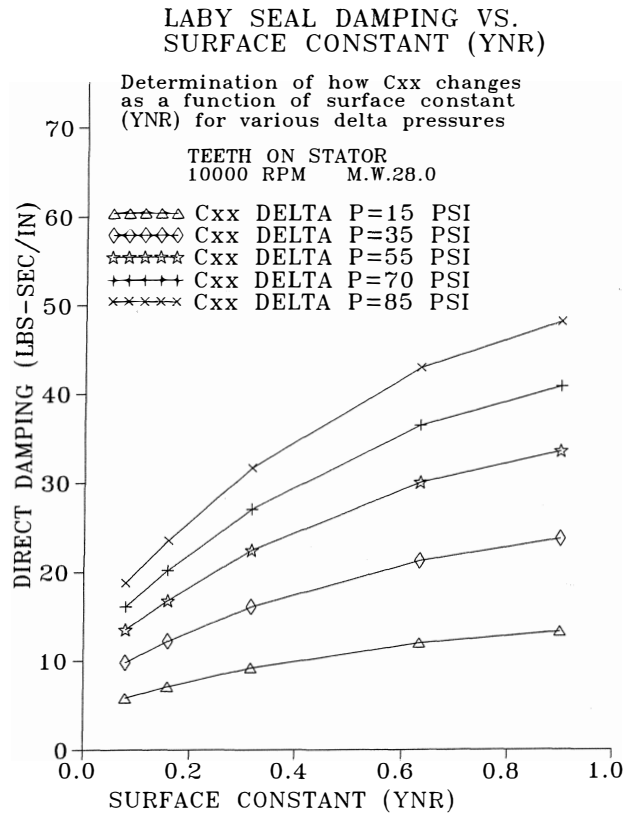

Figure 19. Labyrinth Seal Direct Damping Vs *Shaft Surface Constant.*

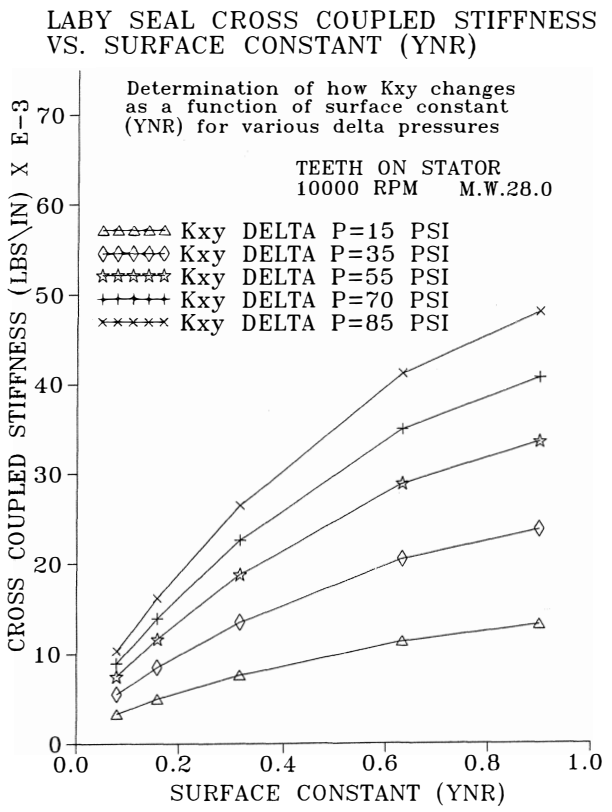

Figure 20. Labyrinth Seal Cross Coupled Stiffness Vs *Shaft Surface Constant.*

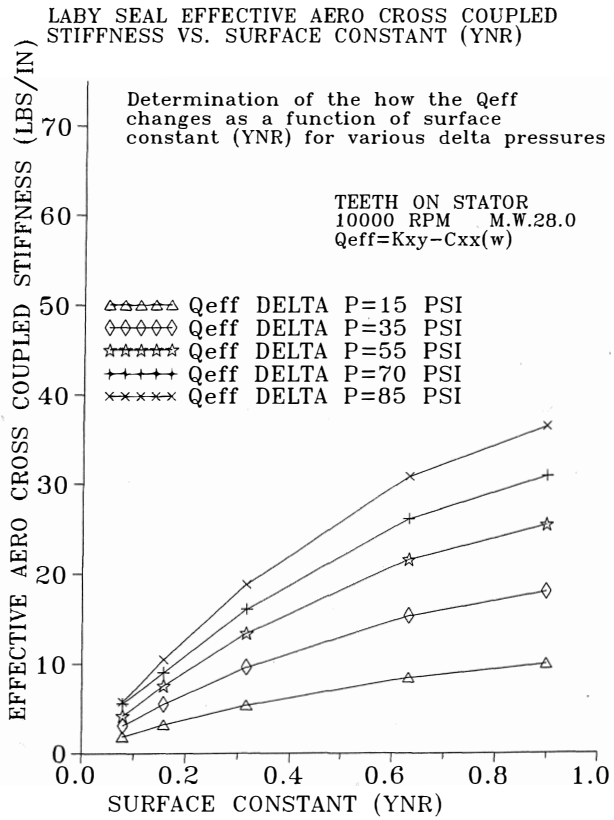

Figure 21. Effective Aero Cross Coupled Stiffness Vs *Shaft Surface Constant.*

damped eigenvalue analysis to determine if the force generated by both seals working together is large enough to drive the rotor unstable for various SFD bearings configurations [8, 9].

DAMPED EIGENVALUE ANALYSIS

The same rotor and bearing models that were used in the synchronous unbalance response were used in the damped eigenvalue analysis [10]. A result of this analysis is the logarithmic decrement of the first natural frequency while the rotor operates at maximum speed as a function of destabilizing force or cross coupled stiffness (K_{xy}). A positive log decrement indicates a stable rotor and a negative log decrement indicates an unstable rotor [11, 12]. The amount of destabilizing force a system can withstand before it becomes unstable is referred to as the stability threshold.

The results of this analysis are documented in Figure 22. Four different bearing configurations were analyzed: 1) standard nondamper bearing, 2) damper bearing with 600 lb-sec/in, 3) damper bearing with 1200 lb-sec/in, and 4) damper bearing with 3600 lb-sec/in. First, with a standard nondamper bearing at zero excitation (K_{xy} = 0), the log decrement of the rotor is positive at about 0.1. As a destabilizing force is applied to the rotor at both labyrinth seal areas, the log decrement of the rotor decreases. For example, as the amount of destabilizing force is raised to 10,000 lb/in, the log decrement becomes negative or unstable. This same technique was applied to the rotor with a damper bearing. The damper bearing increases the amount of destabilizing forces the system can withstand before the rotor goes unstable. For example, a damper bearing with a damping value of 3600 lb-sec/in has a stability threshold of 13,500 lb/in. The stability threshold of this system is 2.7 times the stability threshold of the non-damper bearing system. Results of this analysis are shown in Table 9 for various SFD bearing damping values.

Table 9. Analytical Damped Eigenvalue Results for Various Dampers.

SFD Stiffness (lb/in)	SFD Damping (lb-sec/in)	Log. Dec. at Zero K_{xy}	K_{xy} (Stability Threshold) Value at Zero Log. Dec. (lb/in)
No Damper	0	0.10	5000.
50,000	3,600.	0.26	13,500.
50,000	1,200.	0.60	28,000.
50,000	600.	1.15	34,000.

The results from Figure 21, which show aerodynamic destabilizing forces for various pressures, are plotted as vertical lines on the passive excitation plot for a YNR = 0.4 (Figure 22). At a case pressure of 30 psig, which corresponds to 15 psi across the seal, the rotor running without dampers is calculated to be unstable, because the destabilizing force generated by the seals is greater than the rotors stability threshold. The rotor running on a SFD with a center cage (damping = 600 lb-sec/in) is predicted to have a stability threshold of 34,000 lb/in which exceeds the seals destabilizing force of 22,000 lb/in at 100 psig case pressure. Hence, this centered SFD bearing configuration is predicted to be stable with 100 psig in the case [13, 14, 15].

Data given in Table 9 can be plotted to create a damper optimization curve which shows the relationship between SFD damping and the stability threshold point (Figure 23). The optimum stability threshold occurs with a SFD damping value for this rotor bearing system between 600 to 800 lb-sec/in, because it yields the highest resistance to destabilizing forces.

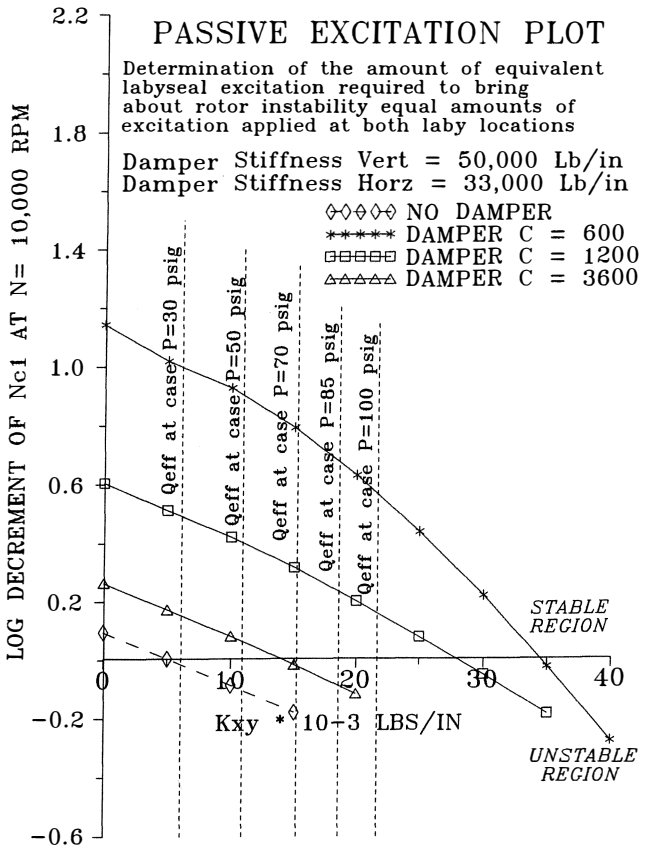

Figure 22. Log Decrement of NC1 Vs Excitation.

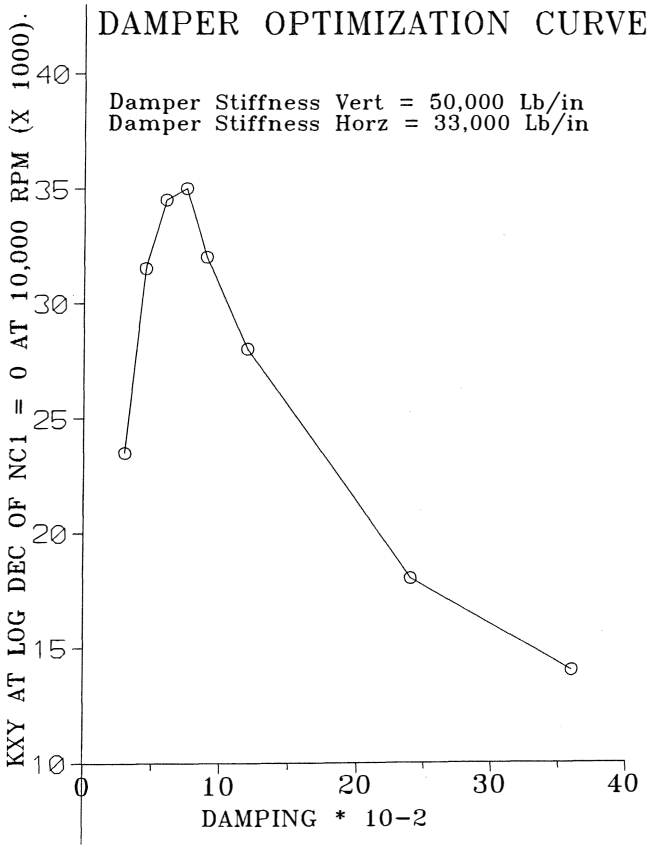

Figure 23. Stability Threshold Damper Optimization Curve.

The SFD bearing designed and tested, as previously discussed, had a centered damping value of 600 lb-sec/in. Similarly, in the synchronous unbalance response work, the optimum damping value for suppressing synchronous vibrations was 600 to 800 lb-sec/in. It is typical to have similar optimum damping values for stability and synchronous unbalance response through the first critical speed [16].

SUBSYNCHRONOUS VIBRATION TEST RESULTS

In this section testing results of the damper configurations previously mentioned will be summarized for tests with 38 psig and 100 psig in the case. Waterfall plots are presented showing frequency sweeps as a function of increasing case pressure at maximum speed.

As in the synchronous vibration test results section, each of the damper configurations tested were subject to the same set of destabilizing forces. This was carried out by using the same labyrinth seals and same pressure across the seals for each damper configuration. This testing is far more interesting than the unbalance response testing because, for some bearing configurations, as pressure is applied violent subsynchronous vibrations erupt. In some cases the testing had to be halted at lower than the 100 psig maximum pressure due to high subsynchronous vibrations (Table 10).

Table 10. Summary of Tests Halted by High Subsynchronous Vibration.

Test Configuration	Max. Pressure Achieved (psig)
No damper	30.
Bottom resting damper	80.
Hanging spring damper with eccentricity= 0.8	60.

Once again, for brevity, the vibration probes discussed include only the free end journal horizontal (FEJH), which measures journal motion relative to the ground, and the midspan horizontal which measures shaft midspan vibration relative to ground.

Test results of subsynchronous vibration at the rotors first natural frequency, while the rotor operates at 10,000 rpm with a case pressure of 38 psig are shown in Table 11.

Table 11. Subsynchronous Vibration Test Results at Low Pressure.

	Eccentricity Ratio e (dim)	FEJH (mil p-p)	Midspan Hor. (mil p-p)
NO Damper	-	1.0*	22.0*
90 viton	0.0	.1	1.0
75 viton	0.6	.05	1.6
90 aflas	0.6	.08	1.1
Bottom Resting	1.0	.18	4.5
Arc spring	0.0	.1	.4
Hanging Spring (centered cage)	0.0	.15	.3
Hanging Spring (above centered cage)	0.8	.3	1.5

*30 psig in the case

These results show, the non damper bearing test was halted at 30 psig when the midspan subsynchronous vibration was measured at 22.0 mil (p-p). As a parametric study, the case pressure was held at 38 psig and all seven SFD bearing designs were tested to compare subsynchronous vibration amplitudes. The bottom resting SFD had 4.5 mil (p-p) of midspan subsynchronous vibrations while the remaining designs all had results between 0.3 mil (p-p) to 1.6 mil (p-p). At this pressure the non damper and bottom resting damper (e = 1.0) clearly showed to be weak designs for the suppression of subsynchronous vibrations. All the other SFD designs with various eccentricity ratios showed comparatively low subsynchronous vibrations. However, as the pressure in the case is increased, larger variations in subsynchronous vibrations are measured due to the differences in stability thresholds for each damper design.

For each of the designs tested, except the standard non-damper design, the speed was held constant at approximately 10,000 rpm and the casing pressure was raised, whenever possible, from 38 psig to 100 psig. Frequency sweeps were taken during these transient conditions in the form of waterfall plots. The standard nondamper bearing design test results are not presented in the same format as the other designs. As the speed was increased to 10,000 rpm, violent subsynchronous vibration amplitudes were measured before the pressure could be increased to 100 psig. Therefore, the results are shown as a cascade plot where the speed is varied at a constant pressure. The nondamper design showed 22.0 mil (p-p) of subsynchronous midspan vibration with 30 psig in the case as shown in Figure 24. A waterfall plot showing the performance of the 75 durometer viton O-ring center SFD (e = 0.6 cage sitting low in the housing) is shown in Figure 25. At 38 psig small amounts of subsynchronous vibration are evident and as case pressure increases up to 100 psig, subsynchronous vibration increased to 3.8 mil (p-p).

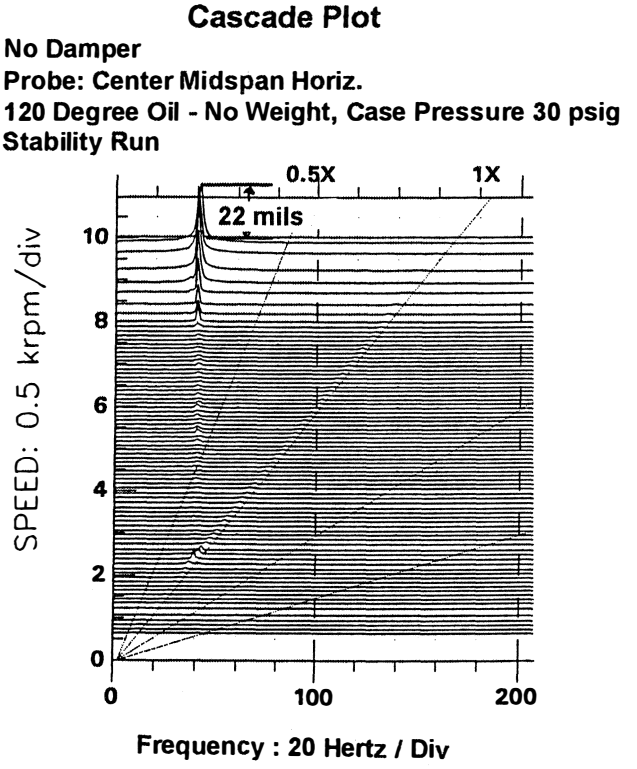

Figure 24. Test Cascade Plot Non Damper.

For the 90 durometer aflas O-ring centered SFD with an eccentricity ratio of 0.6 (cage sitting high in the housing), subsynchronous vibration levels were low with 38 psig in the case. As the pressure increased to 100 psig, the subsynchronous vibration increased to 12.0 mil (p-p) as shown in Figure 26.

Next, the 90 durometer viton O-ring centered SFD with an eccentricity ratio of 0.0 was tested and the results are shown in Figure 27. As the pressure increased from 38 psig to 100 psig minimal changes in subsynchronous vibration were evident.

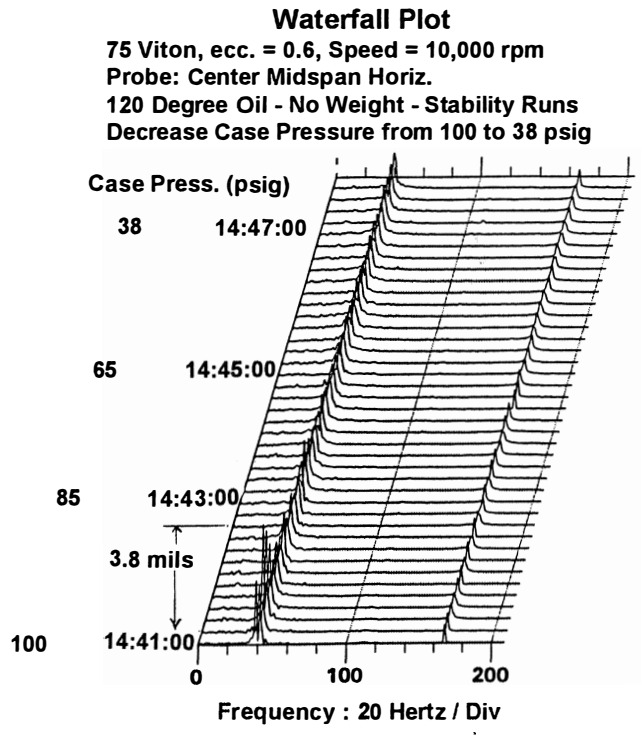

Figure 25. Test Waterfall Plot 75 viton O-Ring Centered SFD e = 0.6.

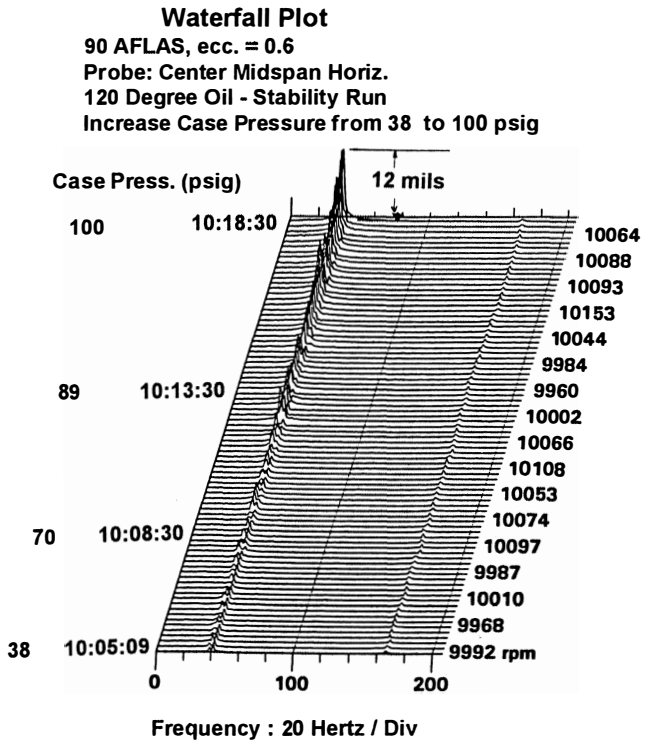

Figure 26. Test Waterfall Plot 90 aflas O-Ring Centered SFD e = 0.6.

For the bottom resting damper with an eccentricity ratio of 1.0, midspan subsynchronous vibration levels increased sharply at 80 psig in the case to 13 mil (p-p) as shown in Figure 28. Hence, testing was halted at this pressure for fear of unbound subsynchronous vibration causing damage to the rig at higher pressures.

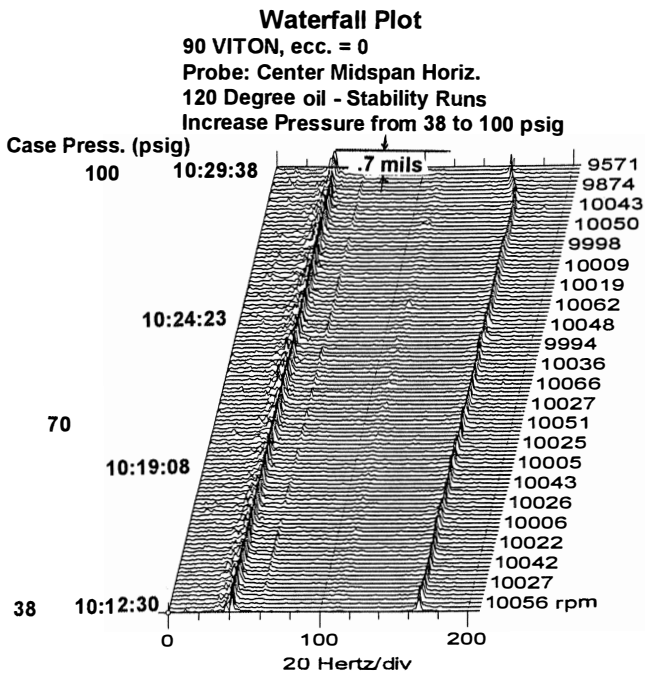

Figure 27. Test Waterfall Plot 90 viton O-Ring Centered SFD e = 0.0.

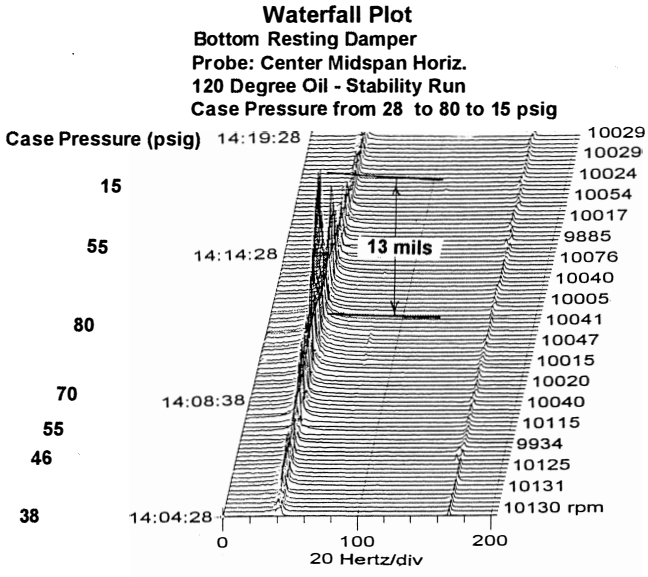

Figure 28. Test Waterfall Plot Bottom Resting SFD e = 1.0.

The arc spring damper assembly, which has an eccentricity ratio of 0.0 showed minimal levels of midspan subsynchronous vibration for all pressure levels tested. The results of the test are shown in Figure 29.

The hanging spring SFD assembly was tested with both an eccentricity ratio of 0.0 and 0.8. First, as shown in Figure 30 with an eccentricity of 0.0, midspan subsynchronous vibration levels remained low with 1.0 mil (p-p) achieved at 100 psig. Next, the bolts of the assembly were turned to raise the cage to an eccentricity ratio of 0.8. The test was rerun and 21.0 mil (p-p) of midspan subsynchronous vibration was measured at 60 psig (Figure 31). Vibrations were such that testing was halted at 60 psig, and a maximum pressure could not be reached. The resolution of this plot shows that within 10 seconds vibrations sky rocketed from

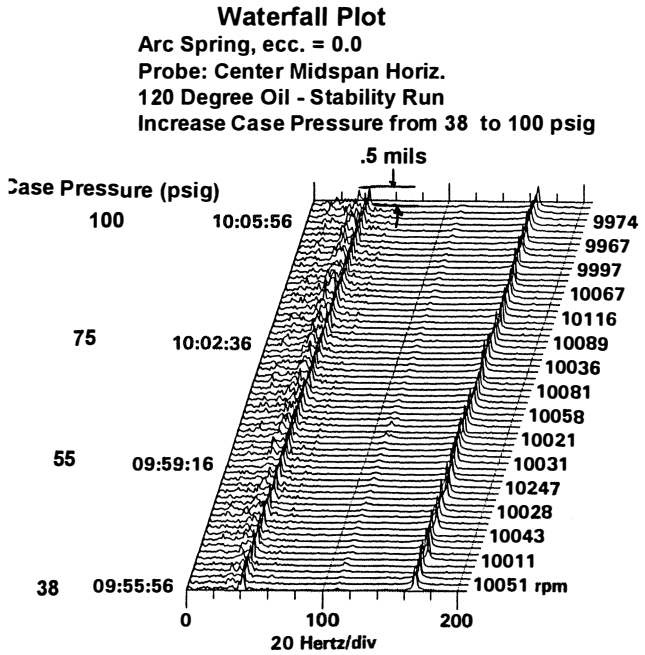

Figure 29. Test Waterfall Plot Arc Spring Supported SFD e = 0.0.

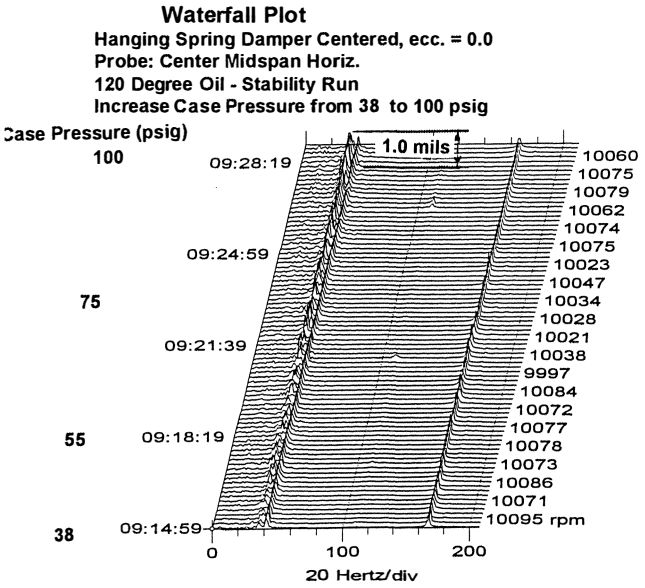

Figure 30. Test Waterfall Plot Hanging Spring Supported SFD e = 0.0.

about 3.0 mil (p-p) to 21.0 mil (p-p) as the pressure increased from 55 to 60 psig. Pressure was immediately backed off and within 10 seconds vibration levels were again under control.

All of the aforementioned subsynchronous vibration levels were measured at the first natural frequency while the rotor operates near 10,000 rpm with 100 psig in the case as summarized in Table 12. To summarize the subsynchronous vibration results, the 90 viton O-ring centered, Arc spring centered and hanging spring centered dampers showed minimal levels of subsynchronous vibrations at 10,000 rpm with 100 psig in the case (e ratio = 0.0). The 90 aflas and the 75 viton O-ring centered dampers do show subsynchronous vibrations at the midspan (e = 0.6). This is likely to be a result of an eccentric cage where an optimum damping was not

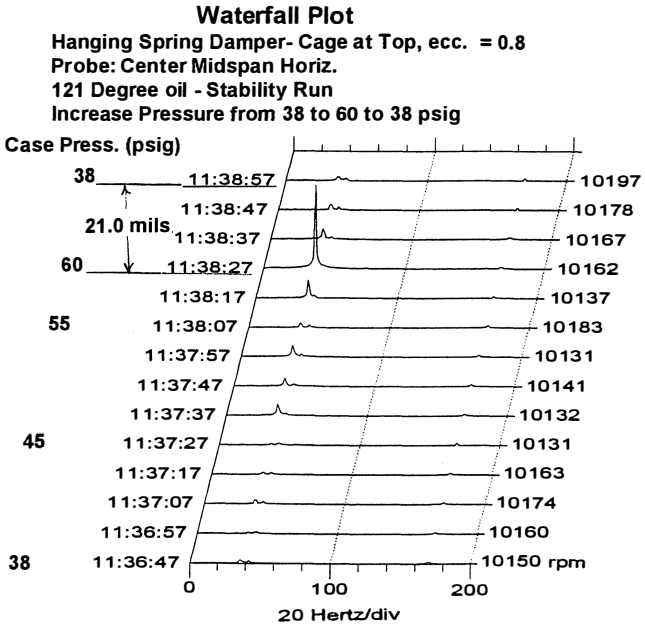

Figure 31. Test Waterfall Plot Hanging Spring Supported SFD e = 0.8.

obtained from the assembly. The bottom resting damper run showed 13.0 mil (p-p) of subsynchronous vibration with 80 psig in the case (e =1.0) while the hanging spring damper run, cage above centerline, showed 21.0 mil (p-p) of subsynchronous vibration with 60 psig in the case(e = 0.8). Finally, The non damper run showed 22.0 mil (p-p) of subsynchronous vibration with 30 psig in the case.

Table 12. Subsynchronous Vibration Test Results at High Pressure.

	Eccentricity Ratio e (dim)	FEJH (mil p-p)	Midspan Hor. (mil p-p)
NO Damper	-	1.0*	22.0*
90 viton	0.0	.05	.7
75 viton	0.6	.16	3.8
90 aflas	0.6	1.2	12.0
Bottom Resting	1.0	.8**	13.0**
Arc spring	0.0	.15	.5
Hanging Spring (centered cage)	0.0	.2	1.0
Hanging Spring (above centered cage)	0.8	5.0***	21.0***

*30 psig in the case
**80 psig in the case
***60 psig in the case

SUMMARY OF SUBSYNCHRONOUS VIBRATION RESULTS/CONCLUSIONS

Each of the bearing assemblies tested was subjected to the same destabilizing force, however in some designs, the maximum case pressure of 100 psig was not achieved because of high subsynchronous vibrations. Nevertheless, the test results show that an eccentric SFD bearing does not perform well, relative to a centered damper to suppress subsynchronous vibration. The more eccentric the cage becomes in the housing the worse the SFD performed. The hanging spring (eccentricity = 0.8) and the bottom resting (e = 1.0) SFD showed very unstable characteristics without achieving maximum destabilizing forces. Furthermore, an O-ring centered damper and a mechanical spring centered damper, both with eccentricities of zero, performed well to suppress subsynchronous vibration.

The three designs tested with eccentricity ratios of 0.0 all performed considerably better than an eccentric damper. Therefore, regardless of how the cage is centered (i.e., O-ring centered or spring centered), if the damper is centered and damping is optimized using the analytical tools available, optimum vibration suppression can be expected.

The analytical damping equation used shows that as eccentricity increases; damping increases. The damped eigenvalue analysis shows that as damping increases above the optimum level; stability threshold decreases. The testing conducted supports these theories and verifies that current damper bearing designs can be analytically predicted to give good correlation with test results.

ACKNOWLEDGMENTS

The authors would like to thank James Brown, Chuck Dunn and Raymond McKinney for testing all of the SFD bearing configurations described herein. In addition, they thank Sean Creeden and Jeff Peer for an outstanding job reducing the data from the rig. We also acknowledge the efforts and suggestions offered by Dresser-Rand's technical staff and finally we thank Dresser-Rand for allowing us to publish this work.

REFERENCES

1. Gunter, E. J., Barrett, L. E., and Allaire, P. E., "Design and Application of Squeeze Film Dampers for Turbomachinery Stabilization," *Proceedings of the Fourth Turbomachinery Symposium,* Turbomachinery Laboratory, Department of Mechanical Engineering, Texas A&M University, College Station, Texas (October 1975).
2. Zeidan, F. Y., "Application of Squeeze Film Dampers," Turbomachinery International, pp. 50-53 (Sept/Oct 1995).
3. Nicholas, J. C., Gunter E. J., and Allaire P. E., "Stiffness and Damping Coefficients for the Five Pad Tilting Pad Bearing," ASME/ASLE Lubrication Conference, Kansas City Missouri, pp. 1-9 (October 1977).
4. Childs, D. W., *Turbomachinery Rotordynamic Phenomena, Modeling and Analysis,* New York, New York: John Wiley and Sons Inc. (1993).
5. Kirk, R. G., "Labyrinth Seal Analysis for Centrifugal Compressor Design–Theory and Practice," Proceedings of the International Conference on Rotordynamics, Tokyo, Japan (September 1986).
6. Kirk, R. G., "A method for Calculating Inlet Swirl Velocity," ASME 11th Biennial Conference on Mechanical Vibration and Noise, Boston, Massachusetts, USA (September 1987).
7. Childs, D. W. and Scharrer, J. K., "An Iwatsubo-Based Solution for Labyrinth Seals–Comparison of Experimental Results," Texas A&M University, College Station Texas, NASA CP 2338, pp. 257-279 (May 1984).
8. Kirk, R. G., "Evaluation of Aerodynamic Instability Mechanisms for Centrifugal Compressors–Part I: Current Theory," Journal of Vibration Stress, and Reliability in Design, *110* (April 1988).
9. Kirk, R. G., "Evaluation of Aerodynamic Instability Mechanisms for Centrifugal Compressors–Part II: Advanced Analysis," Journal of Vibration Stress, and Reliability in Design, *110* (April 1988).
10. Lund, J. W., "Stability and Damped Critical Speeds of a Flexible Rotor in Fluid Film Bearings," ASME, Journal of Engineering for Industry, *96,* (2), pp. 509-517 (May 1974).
11. Vance J. M., *Rotordynamics of Turbomachinery,* New York, New York: John Wiley and Sons Inc. (1988).
12. Rabinowitz, M. D. and Hahn, E. J., "Stability of Squeeze Film Damper Supported Flexible Rotors," Journal of Engineering for Power Trans. ASME, Series A, *99,* (4), pp. 545-551 (1977).
13. Memmott, E. A., "Damper Bearings and Stability of a CO2 Compressor," Seventh Annual Rotating Machinery and Controls Industrial Research Conference, San Diego, California (June 1987).
14. Marshall, D. F., Hustak, J. F., and Memmott, E. A., "Elimination of Subsynchronous Vibration Problems in a Centrifugal Compressor by the Application of Damper Bearings, Tilting Pad Seals, and Shunt Holes," Eastern Regional Machinery Conference, ASME (November 1993).
15. Memmott, E. A., "Stability of Centrifugal Compressors by Application of Tilt Pad Seals, Damper Bearings, and Shunt Holes," IMechE, Fifth International Conference on Vibrations in Rotating Machinery, Bath, England (September 1992).
16. Barrett, L. E., Gunter, E. J., and Allaire, P. E., "Optimum Bearing Support Damping for Unbalance Response and Stability of Rotating Machinery," Trans. ASME, Journal of Eng. for Power, pp. 1-6 (1978).